This is a post-peer-review, pre-copyedit version of an article published in Nature Astronomy.
The final authenticated version is available online at https://www.nature.com/articles/s41550-021-01380-6

Possible observational evidence that cosmic filaments spin

Peng Wang[1*], Noam I. Libeskind[1,2*], Elmo Tempel[3], Xi Kang[4,5], Quan Guo[6]

Most cosmological structures in the universe spin. Although structures in the universe form on a wide variety of scales from small dwarf galaxies to large super clusters, the generation of angular momentum across these scales is poorly understood. We have investigated the possibility that filaments of galaxies - cylindrical tendrils of matter hundreds of millions of light-years across, are themselves spinning. By stacking thousands of filaments together and examining the velocity of galaxies perpendicular to the filament's axis (via their red and blue shift), we have found that these objects too display motion consistent with rotation making them the largest objects known to have angular momentum. The strength of the rotation signal is directly dependent on the viewing angle and the dynamical state of the filament. Just as it is easiest to measure rotation in a spinning disk galaxy viewed edge on, so too is filament rotation clearly detected under similar geometric alignment. Furthermore, the mass of the haloes that sit at either end of the filaments also increases the spin speed. The more massive the haloes, the more rotation is detected. These results signify that angular momentum can be generated on unprecedented scales.

SDSS DR12

Филаменты аппроксимировались цилиндрами, включались галактики в пределах 2Мпк от филамента

3 бина по углу наклона к лучу зрения: все филаменты, >60^o, >80^o

$\Delta z_{AB} = z_A - z_B$; z_{rms}

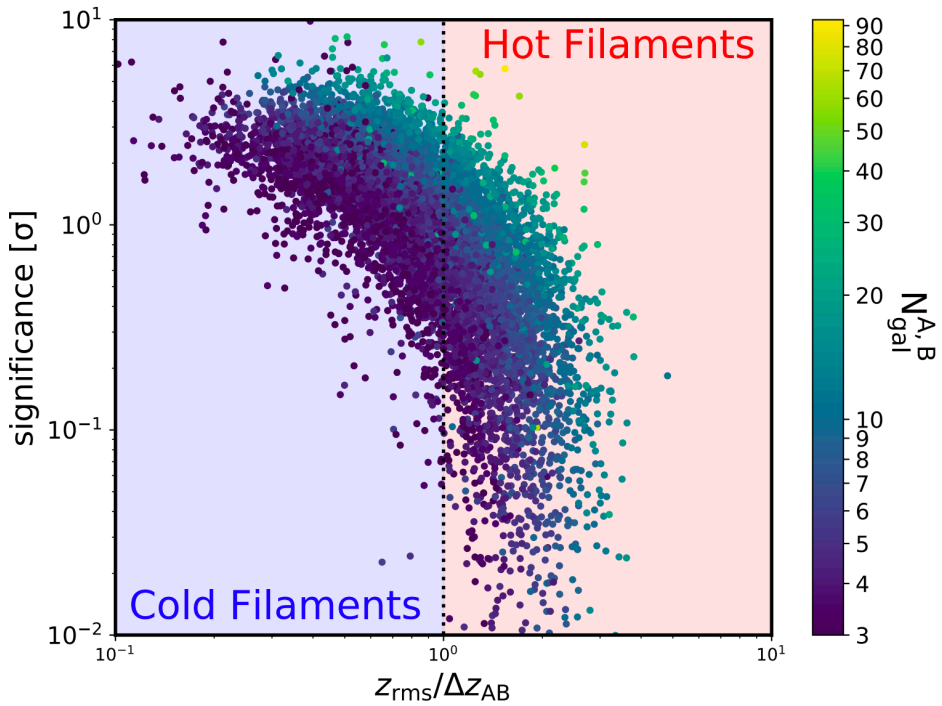

Figure 1 – The statistical significance of Δz_{AB} being consistent with random is shown as a function of the filament dynamical "temperature", $z_{rms}/\Delta z_{AB}$, in which Δz_{AB} is the redshift difference of galaxies between the approaching and receding regions of each filament. The higher this quantity, the more unlikely it is that Δz_{AB} is a random occurrence. Each filament is colored codes by the number of galaxies it contains, with yellow being rich filaments and purple being poor filaments as designated by the color bar. At a given value of $z_{rms}/\Delta z_{AB}$, the Δz_{AB} seen in richer filaments is more statistically inconsistent with random. 'Cold' or 'hot' filaments are separated by $z_{rms}/\Delta z_{AB} = 1$.

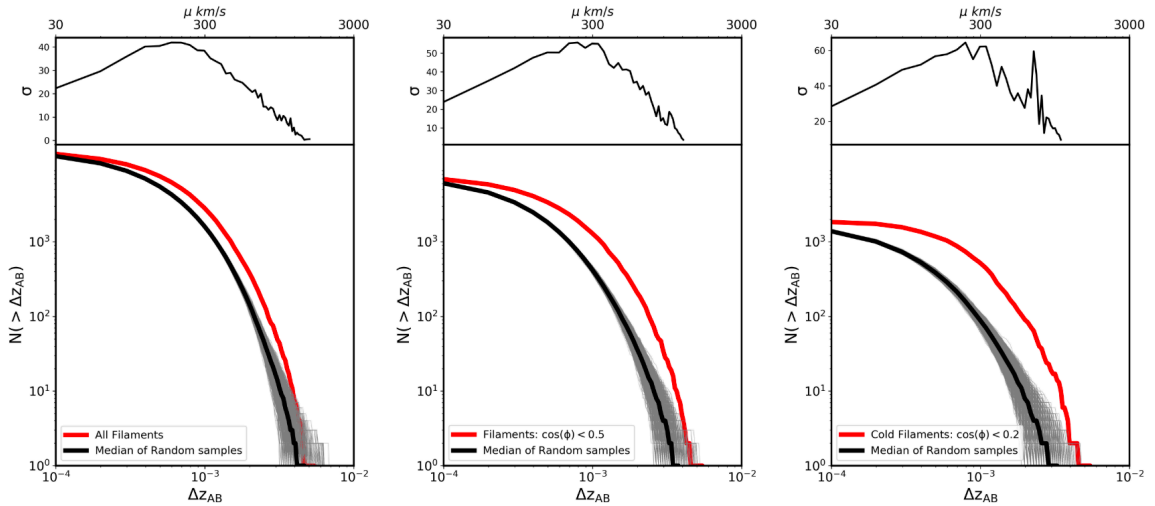

Figure 2 – The cumulative distribution of Δz_{AB} , the redshift difference of galaxies in the approaching and receding regions of each filament. Left panel: all filaments irrespective of viewing angle. Middle panel: filaments whose axis subtends an angle $\cos\phi < 0.2$ with the line of sight. Right panel: filaments whose axis subtends an angle $\cos\phi < 0.5$ with the line of sight and which are dynamically cold, namely $z_{rms}/\Delta z_{AB} < 1$. The red solid line shows the distribution of observed filaments, while the 10,000 grey lines indicate the expected distribution from randomized redshifts. The median value of these 10,000 random samples is shown as the black solid line. The upper panels measure, as a function of Δz_{AB} , the distance, in units of the standard deviation of the randomized distribution, between the measured curve and the mean of the random distributions. The upper x-axis displays the rotation velocity of the filament in km/s calculated as $\mu = c \times \Delta z_{AB}$.

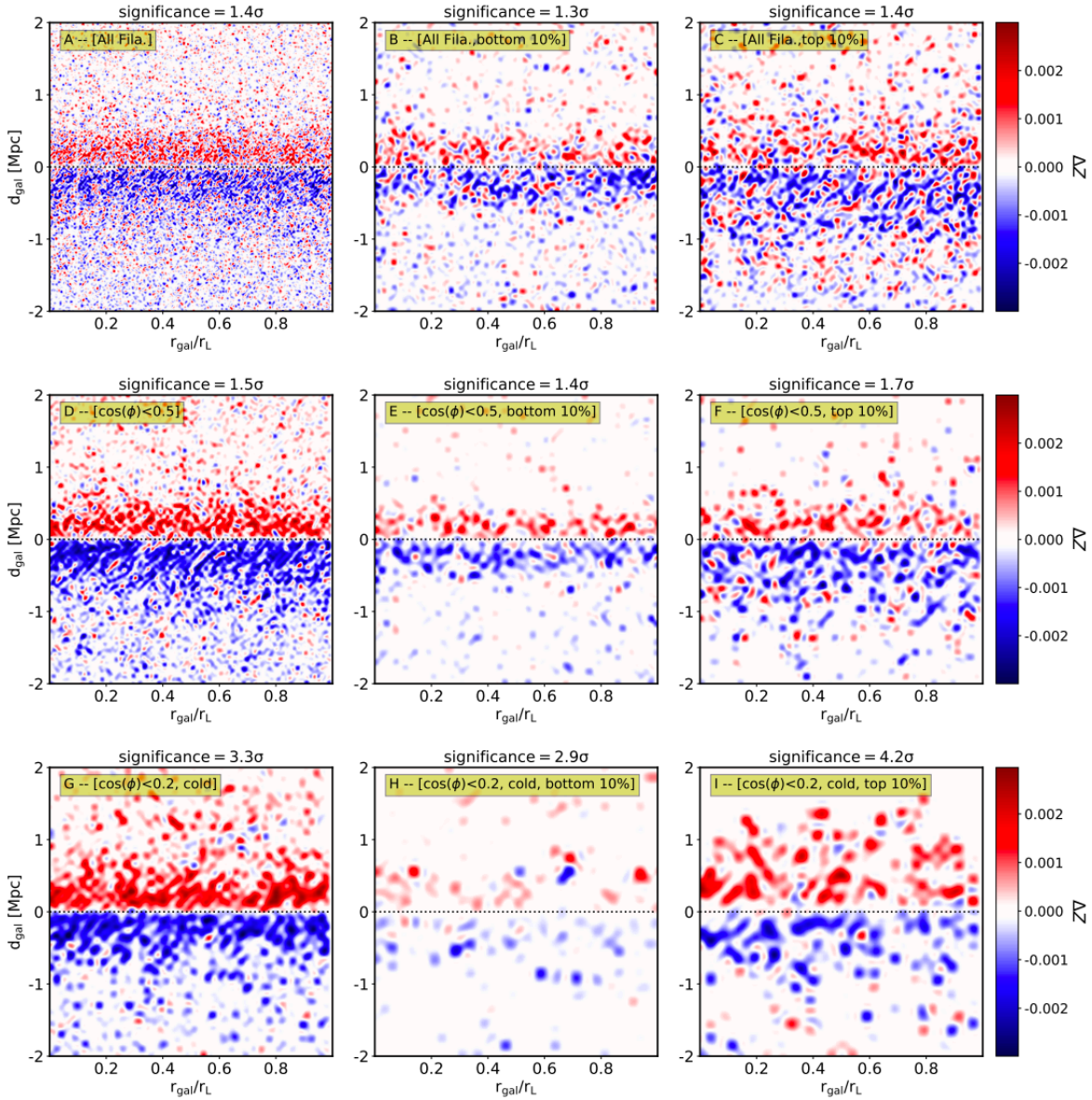

Figure 3 – The stacked rotation signal of filaments. Galaxies' position $r_{\rm gal}$ long the filament are scaled by the length $r_{\rm L}$ of the filament. $d_{\rm gal}$ is the distance of galaxies to the filament axis. Region A (defined as the region with greater mean redshift) is shown in the upper part of each plot, while region B is shown in the lower part. From top to bottom, each row shown the stacked rotation signal for all filaments, filaments whose spine subtend an angle $cos(\phi) < 0.5$ with the line of sight and filament with $cos(\phi) < 0.2$ and which have $z_{\rm rms}/\Delta z_{\rm AB} < 1$. These three samples of filaments are subdivided according the group mass they are point to. Middle and right columns show the stacked rotation signal for filaments with the smallest and largest 10 percentile filament end point mass. The redshift difference is coded in color bar.

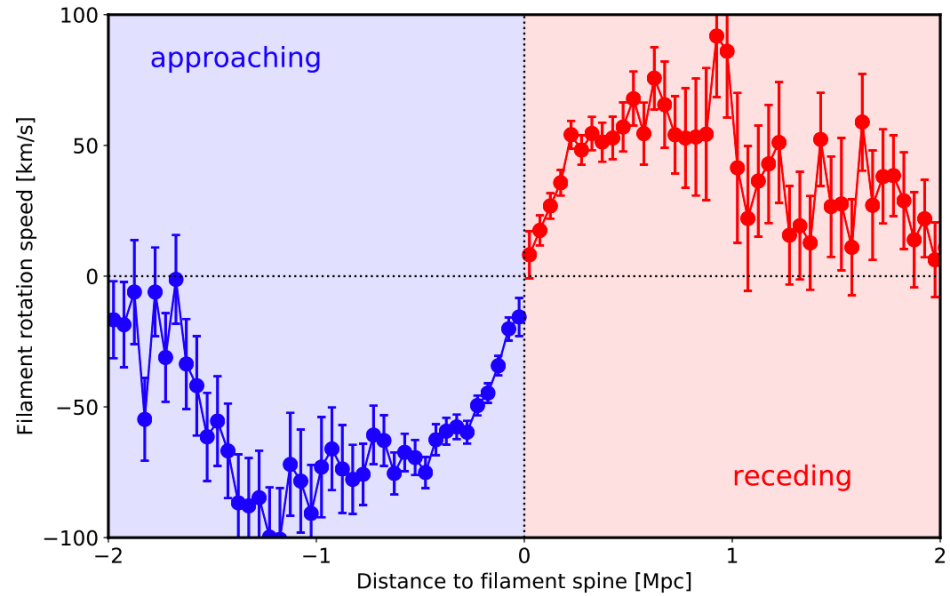

Figure 4 – The rotation curve of filaments as a function of the distance between galaxies to filament spine. The rotation speed is calculate by $c \times \Delta z_i$, where Δz_i is the redshift difference of galaxies at given distance with respect to the mean redshift of all galaxies in the filament. The distance of galaxies in the region A (or receding region, defined as the region with greater mean redshift) is marked as positive values, while the distance of galaxies in the region B (or approaching region, defined as the region with smaller mean redshift) is marked as negative values. Error bars represent the standard deviation about the mean.

Origin of stellar prolate rotation in a cosmologically simulated faint dwarf galaxy

Salvador Cardona-Barrero,[1,2]★ Giuseppina Battaglia,[1,2] Arianna Di Cintio,[2,1]† Yves Revaz[3] & Pascale Jablonka[3,4]

[1]*Instituto de Astrofísica de Canarias, Calle Via Láctea s/n, E-38206 La Laguna, Tenerife, Spain*
[2]*Universidad de La Laguna. Avda. Astrofísico Fco. Sánchez, La Laguna, Tenerife, Spain*
[3]*Institute of Physics, Laboratoire d'astrophysique, École Polytechnique Fédérale de Lausanne (EPFL), Observatoire, CH-1290 Versoix, Switzerland*
[4]*GEPI, Observatoire de Paris, Université PSL, CNRS, Place Jules Janssen, F-92190 Meudon, France*

Accepted XXX. Received YYY; in original form ZZZ

ABSTRACT

Stellar prolate rotation in dwarf galaxies is rather uncommon, with only two known galaxies in the Local Group showing such feature (Phoenix and And II). Cosmological simulations show that in massive early-type galaxies prolate rotation likely arises from major mergers. However, the origin of such kinematics in the dwarf galaxies regime has only been explored using idealized simulations. Here we made use of hydrodynamical cosmological simulations of dwarfs galaxies with stellar mass between 3×10^5 and 5×10^8 $M_\odot$ to explore the formation of prolate rotators. Out of 27 dwarfs, only one system showed clear rotation around the major axis, whose culprit is a major merger at $z = 1.64$, which caused the transition from an oblate to a prolate configuration. Interestingly, this galaxy displays a steep metallicity gradient, reminiscent of the one measured in Phoenix and And II: this is the outcome of the merger event that dynamically heats old, metal-poor stars, and of the centrally concentrated residual star formation. Major mergers in dwarf galaxies offer a viable explanation for the formation of such peculiar systems, characterized by steep metallicity gradients and prolate rotation.

High-resolution, zoom-in cosmological hydrodynamical simulations

Звезды+газ+темная материя

-> 27 карликов (массы звезд от $3*10^5$ до $5*10^8$, что соответствует LG dwarfs), 1 показывает prolate rotation

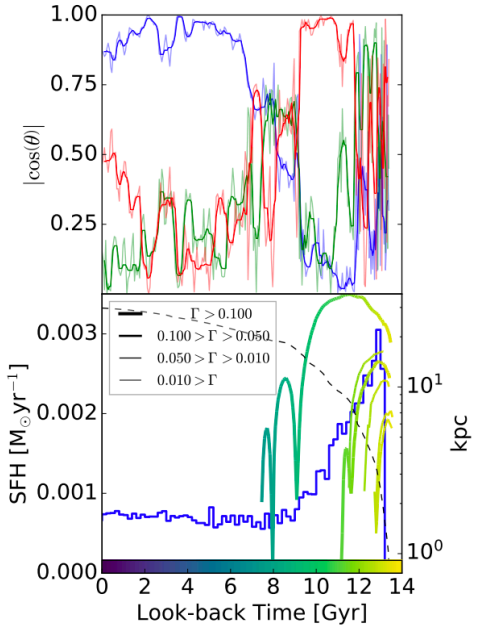

Figure 1. Top: Principal Axes orientation with respect to the stellar angular momentum as a function of look-back time. The major, minor and intermediate axis are shown in blue, red and green respectively. We show the values obtained from individual snapshots (thin lines) and a running average (thick lines) using a window of 6 snapshots (∼ 0.34 Gyrs). Bottom: SFH (blue) and dark matter halo virial radius (black dashed line) of h048, together with the orbits of infalling satellites, color-coded by look-back time (the width of the lines has been set depending on the total mass ratio Γ between the main progenitor and the satellite, measured at the snapshot when the satellite first crosses the main progenitor's virial radius). The SFH is similar to the one found in Phoenix (Gallart et al. 2015). Note that the gas mass of the satellite is negligible with respect to that of the host (see Tab. 1), being the effect on the SFH imperceptible.

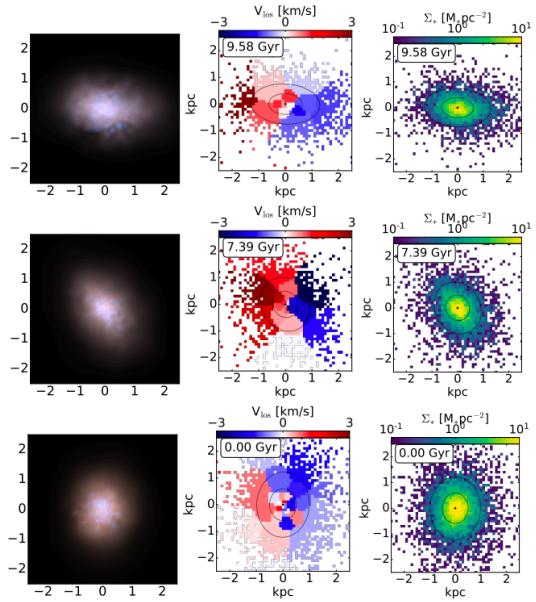

Figure 2. Properties of h048 projected onto the line-of-sight. From left to right: RGB rendering of the stellar particles combining the I, V and B filters following the procedure described in Lupton et al. 2004; line of sight stellar velocity field; projected stellar density. Top: The main progenitor of the galaxy at 9.58 Gyrs (before the merger). Middle: The main progenitor of the galaxy at 7.39 Gyrs, at this time the main progenitor and the satellite are fully merged. Bottom: galaxy at redshift 0. The line of sight has been chosen to be perpendicular to the stellar angular momentum, which is aligned with the Y-axis in the projected maps. The stellar particles are distributed in a grid with 0.1 kpc-wide bins. The velocity field has been constructed using the Voronoi tessellation algorithm of Cappellari & Copin 2003 ensuring a minimum number of 200 star particles in each Voronoi bin. The velocity of each bin corresponds to the mass weighted average of the velocities of the stars belonging to the bin. The ellipses in the velocity and density maps indicate 1 and 2 half mass radius.

	Host $z = 0$	Host $z = 1.78$	Satellite $z = 1.78$
$M_{vir}/M_\odot$	2.8×10^9	1.6×10^9	3.4×10^8
$M_*/M_\odot$	1.4×10^7	6.5×10^6	2.4×10^5
$M_{gas}/M_\odot$	2.3×10^7	4.0×10^7	9.1×10^4
$(L_{Major}/L_{Tot})^2$	0.780	0.040	0.004
$V_{rot}^{max}/\langle\sigma_{3D}\rangle$	0.19	0.30	0.33
b/a	0.76	0.64	0.68
c/a	0.70	0.49	0.51
$r_{1/2}$/kpc	0.70	0.64	0.62
$R_{1/2}$/kpc	0.57	0.48	0.42

Table 1. Properties of h048 at z=0 (left) and at $z = 1.78$ (middle), corresponding to its main progenitor just before the merger analyzed; properties of the accreting satellite at $z = 1.78$ (right). We include the virial mass M_{vir}, the stellar mass M_*, the total gas mass M_{gas}, the ratio between the angular momentum of the stellar component parallel to the major axis and the total angular momentum (L_{Major}/L_{Tot}), the rotation velocity at 2 kpc divided by the $3D$ velocity dispersion $\sigma_{3D}^2 = \sum_i^3 \sigma_i^2/3$, the axis ratios b/a and c/a, and the 3D and projected stellar half mass radii $r_{1/2}$ and $R_{1/2}$.

По сравнению с пред. модельными работами:

- Малые массы
- Удается воспроизвести градиент металличности
- Нету строгих ограничений на ориентацию орбит
- Во взаимодействии участвуют сфероидальные системы

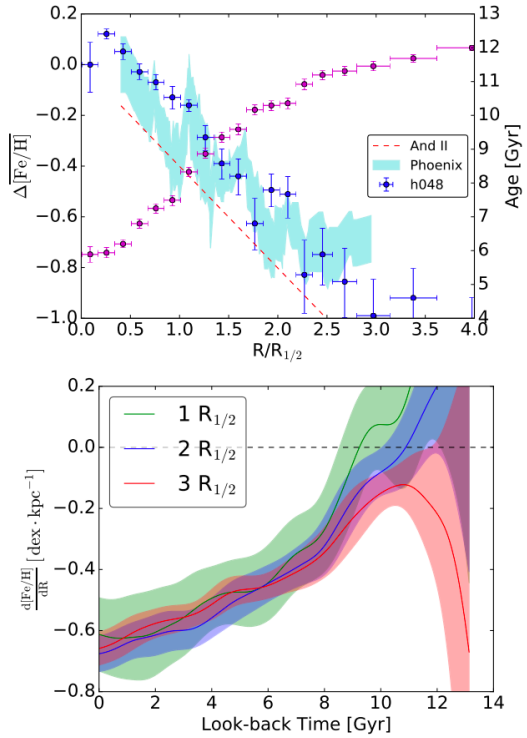

Figure 3. Top panel: Average age (magenta) and metallicity (blue) projected radial profiles of h048, with the latter normalized to its central value. The error-bars correspond to the standard error of the average. The radial coordinate has been normalized to the half mass radius in order to compare with the metallicity profiles of the Phoenix (Kacharov et al. 2017) and Andromeda II (Ho et al. 2015) galaxies, in light-blue and dashed red respectively. Bottom panel: the evolution of the metallicity gradient of the simulated galaxy as a function of look-back time, computed within 1, 2 and 3 effective radii (green, blue and red respectively). The profiles have been smoothed via a Gaussian with standard deviation of 0.5 Gyrs. The shaded regions correspond to the 1σ uncertainty over the smoothed evolution.

Не удается воспроизвести вращение наблюдаемых галактик. Но моделируются изолированные системы.